Korean J. Chem. Eng., 35(3), 671-683 (2018)
DOI: 10.1007/s11814-017-0293-9

pISSN: 0256-1115
eISSN: 1975-7220

Mercury ion adsorption on AC@Fe_3O_4-NH_2-COOH from saline solutions: Experimental studies and artificial neural network modeling

Mohammad Pazouki*,†, Mohammad Zabihi,***, Jalal Shayegan****, and Mohammad Hossein Fatehi****

*Laboratory of Electrochemistry, Materials and Energy Research Center, P. O. Box 14155-4777, Tehran, Iran
**Chemical Engineering Faculty, Sahand University of Technology, P. O. Box 51335-1996, Sahand New Town, Tabriz, Iran
***Environmental Engineering Research Center, Sahand University of Technology, Tabriz, Iran
****Department of Chemical and Petroleum Engineering, Sharif University of Technology, Azadi Avenue, P. O. Box 11155-9465, Tehran, Iran
(*Received 17 June 2017 • accepted 15 October 2017*)

Abstract−An efficient, novel functionalized supported magnetic nanoparticle (AC@Fe_3O_4-NH_2-COOH) has been synthesized by co-precipitation method for removal of mercury ions from saline solutions. High dispersed supported magnetic nanoparticles with particle sizes less than 30 nm were formed over activated carbon derived from local walnut shell. Surface characterizations of supported magnetic nanoparticles were evaluated by Boehm test, Brunauer-Emmett-Teller (BET) surface area, X-ray diffraction (XRD), transmission electron microscopy (TEM), Fourier transform infrared spectroscopy (FT-IR), thermogravimetric analysis (TGA) and X-ray fluorescence (XRF). A three-layer artificial neural network (ANN) code was developed to predict the Hg (II) ions removal from aqueous solution by AC@Fe_3O_4-NH_2-COOH. The three-layer back-propagation (BP) is configured of tangent sigmoid transfer function (tansig) at hidden layer with eight neurons for AC@Fe_3O_4-NH_2-COOH, and linear transfer function (purelin) at output layer. According to the calculated MSEs, Levenberg-Marquardt algorithm (LMA) was the best training algorithm among others. The linear regressions between the predicted and experimental outputs were proven to be a good agreement with a correlation coefficient of about 0.9984 for five model variables. Maximum adsorption capacity was achieved 80 mg/g by Langmuir isotherm at pH of 7 and salinity of 25,000 ppm. Kinetic studies illustrated that mercury adsorption follows pseudo-second-order.

Keywords: Adsorption, Mercury-magnetic, Salinity, Activated Carbon, Co Precipitation, Artificial Neural Network

INTRODUCTION

Adsorption of mercury ions (II) from aqueous solutions by nanoparticles adsorbents is an efficient, low operating cost technique among other treatment technologies [1]. The existence of mercury ions is of main environmental relevance for much industrial wastewater. Mercury is an important material widely employed in the electrical industry, petrochemical plants, chlorine production and laboratories [2,3]. It can damage the blood, kidney, central nervous system, and cause cancer in humans [2]. Generally, industrial wastewater exhausted to the sea contains a mixture of contaminants and salinity, and a significant issue is the simultaneous adsorption of different ions and interaction between ions over adsorbents [4,5]. Adsorbents for adsorption process can be categorized as magnetic and non-magnetic materials, which can also be categorized in terms of carbonaceous and non-carbon materials. Various materials such as activated carbons [2,3], alumina [6-8], zeolite [9-11], and silica [12-14] have been utilized as an adsorbent for removal of heavy metal ions from solutions.

Activated carbon as an adsorbent has several advantages including hydrophobicity, high surface area, low cost, and flexible surfaces and different low priced raw materials can be applied for preparing it [15]. Many studies have focused on using non-magnetic and carbon adsorbents for removal of mercuric ions, but most of them have some drawbacks, including low adsorption efficiency, low surface area, and high cost of use and difficulty of separation from treated solutions [2,3]. Based on previous investigations, there are a few studies on adsorption of mercury ions by using supported magnetic nano-particles on activated carbons [16,17]. There are also some stringent standards and restrictions for industrial discharges.

Therefore, it is necessary to develop a suitable model which provides a desirable tool in controlling the adsorption, and developing a continuous control strategy for management of this simultaneous adsorption that helps to describe the real process performance. Since modeling a process with ANNs needs no precise information of the adsorption, there has been growing interest in this technique for modeling processes which are not exactly known [18-20]. ANNs are very beneficial because they do not need to allocate so much time like traditional mathematical models. They have been successfully conducted in the past decade, such as estimation of lead concentration [21] and physicochemical wastewater treatment [22,23]. ANNs have been used in different parts of environmental engineering fields because of their high quality in computing the non-linear relationships between variables in complex systems.

†To whom correspondence should be addressed.
E-mail: mpazouki@merc.ac.ir

Our main aim here was to design and synthesize a novel and appropriately supported magnetic nanoparticles by conventional co-precipitation method on the activated carbon derived from Iranian walnut shell. Furthermore, the influence of salinity was studied on the adsorption of mercury ions over prepared supported magnetic nanoparticles. Role of several important operating parameters, such as salinity, pH solution, adsorption temperature, initial concentration of mercury ions, was determined in this present study. Neural network modeling was implemented for the prediction of mercury removal from aqueous solution by experimental data from the performance of the prepared magnetic adsorbent.

MATERIALS AND METHODS

1. Preparation of Adsorbent

All chemicals and reagents including $HgCl_2$, $FeCl_3{\cdot}6H_2O$, $FeCl_2{\cdot}4H_2O$, 3-aminopropyl triethoxysilane (APTMS), succinic anhydride, N, N-dimethylformamide (DMF), NaOH, KOH were provided from Merck Company. Initially, the activated carbon derived from walnut shell was prepared in tubular furnace by physical activation method with water vapor as a chemical agent at 800 °C.

Magnetic nanoparticles (MNPs) supported on walnut shell activated carbon were prepared by conventional co-precipitation method. 80 mmol of $FeCl_3{\cdot}6H_2O$ and 40 mmole of $FeCl_2$. According to analytical and stoichiometric computations, purchased salts were dissolved in 600 ml deionized water using mechanical stirring at 70 °C for 2 hour. Thereafter, 10 g of the powdered walnut shell activated carbon (mesh no. 100 and below) was added to achieve AC-Fe_3O_4 weight ratios of 1 : 1 (activated carbon: Fe_3O_4). Then, the solution was slowly stirred for one hour under nitrogen flow as a carrier and the inert gas.

To form the black product of AC-MNPs, 5 M aqueous NaOH (6% wt) was added by rate of 0.05 ml/s into the suspension to reach pH of 10-11 for one hour. Precipitate was collected by magnetic separation after 24 hour aging at ambient temperature and frequently washed with warm distilled water and ethanol dilution, then dried at 50 °C overnight.

Amino-functionalized AC-MNPs was synthesized by dispersing 2 g of AC@Fe_3O_4 into a heated 200 ml of ethanol-water (1 : 1) solution at 70 °C under an argon flow. 5 ml of 3-aminopropyl triethoxysilane was added dropwise to the solution in the presence of the constant argon flow, and the mixture pH was adjusted to 11.0 by adding KOH solution. After 5 h mixing, the amino-functionalized MACNPs was magnetically separated and repeatedly washed with distilled water to remove any undesirable materials and then dried at 50 °C overnight.

Finally, the AC@Fe_3O_4-NH_2 was stirred with 10% succinic anhydride in N,N-dimethylformamide solution under argon flow at room temperature for 5 hours. AC@Fe_3O_4-NH_2-COOH was magnetically separated and repeatedly washed with distilled and then dried at 50 °C overnight [24].

2. Adsorbent Characterizations

Boehm test was applied for assessment of the surface functional groups of samples [2]. Surface area of the samples was determined from monolayer nitrogen (N_2) adsorption and desorption isotherms at 77 K using an ASAP-1100 Micromeritics equipment. The specific surface area of porous adsorbent was calculated using the Brunauer-Emmett-Teller (BET) and t-plot theories [3]. The pore volume was calculated from the amount of N_2 adsorbed at a relative pressure of 0.99. X-ray diffraction (XRD) patterns for the prepared samples were performed using model D-64295 equipment from STOE Company. XRD analysis was at 30 kV, 20 mA, copper Kα radiation and scanning rate of 3°/min. The size distribution profile of MNPs was determined by dynamic light scattering (DLS) by Nano AS (red badge) ZEN 3600 from UK. The products for transmission electron microscopy (TEM) micrographs were obtained by CM30-Philips instrument equipped with a Schottky field emission gun operated at 150 keV to determine the morphology and element distribution of nanoparticles. Moisture, ash and oxidation resistance of prepared magnetic support was studied by thermogravimetric analysis (TGA) using by TGA-25 apparatus, Mettler Toledo Switzerland, while heating the sample up to 1,000 °C, under airflow of 55 ml/min and heating rate of 10 °C/min. Fourier transform infrared spectroscopy (FT-IR, Nicolet IS10) was implemented to analyze the molecular structure of the prepared magnetic particles at a resolution of 4 cm^{-1}. To determine the chemical elements of the magnetic adsorbent, X-ray fluorescence was applied by Spectro-Xepos device from Germany.

3. Batch Adsorption Studies

Adsorption of mercury ions in saline solution over the supported magnetic nanoparticles denoted by AC@Fe_3O_4-NH_2-COOH was studied using batch experiments within the pH range of 2 to 11 while the adsorption temperature (25, 35 and 45 °C) was adjusted to desired values by heater as follows. Stock solutions of mercury ions were prepared by dissolving a sufficient amount of $HgCl_2$ in deionized water and diluted to obtain the desired concentrations prior to adsorption experiments. To evaluate the effect of salinity on removal of mercuric ions by prepared nanoparticles, experiments were accomplished under various NaCl concentrations (1,000, 10,000, 20,000 and 30,000 ppm) in mercury ions solutions, which are close to the salinities of seawater.

Each adsorption study was run with 0.05 g sample and 50 ml of simulated contaminated solution with the desired concentration in two conical flasks, simultaneously. The solutions, including nanomagnetic adsorbent and adsorbate, were agitated and heated for predetermined time intervals using a mechanical shaker with 600 rpm velocity.

At the end of agitation, the magnetic particles were gathered with permanent hand-held magnet and filtration. The amount of metal ions in the final 25 ml volume was measured by atomic absorption spectrophotometer (Varian, spectra-110-220/880 Australia Pty. Ltd.) equipped with a Zeeman atomizer. The obtained outputs for two similar solutions with no significant differences were averaged and reported. Removal efficiency of metal ions was calculated by equation as follows:

$$RE = \frac{(C_o - C_e)}{C_o} \times 100 \quad (1)$$

where RE is removal efficiency, C_o and C_e (mg/*l*) are initial and outlet concentration, respectively.

4. Artificial Neural Network

Neural network was employed in this investigation due to more

benefits in simulation and prediction of adsorption process. Significant advantages of ANN are that there is no need for mathematical description of the phenomena. ANN consists of several individual processing units called neurons, which are inspired from the human brain biology.

We used a three layer back-propagation neural network with tangent sigmoid transfer function (tansig) at hidden layer and a linear transfer function (purelin) at output to simulate the mercuric adsorption on AC@Fe_3O_4-NH_2-COOH. Back-propagation algorithm was applied due to performing network training. To predict mercury removal adsorption, an ANN code was written in Matlab Version (2014 a). Obtained data from these experiments (69 experimental sets for each carbon) were divided into two matrices, one as input [P] and the other as target [T].

Too find important variables to be set as the input, principal component analysis (PCA) was performed as an effective procedure. The principal components were conservatively preserved, which accounts for 99.9% of the variation in the data set. Due to PCA, the data sets were divided to the validation set (20%), test set (20%) and training set (60%).

RESULTS AND DISCUSSION

1. Characterization

The amounts of acidic and basic groups of AC@Fe_3O_4 and AC@Fe_3O_4-NH_2-COOH containing phenolic, lactonic, carboxylic, and basic groups are measured in Table 1 by the Boehm test. Significant amounts of acidic groups (1.48 mequiv./g) that are representative of oxygen groups on the surface of AC@Fe_3O_4-NH_2-COOH make the prepared magnetic nanoparticles adsorbent appropriate for deep adsorption of mercury from saline solutions [25]. Results from Table 1 show that AC@Fe_3O_4 with insignificant amounts of oxygen groups was modified by adding various functional groups during synthesis method.

Material type and oxidation resistance of AC@Fe_3O_4 and AC@Fe_3O_4-NH_2-COOH are illustrated in Fig. 1 using TGA test. There was no oxidation below 200 °C for magnetic nanoparticles over activated carbon due to the vaporization of water in two samples. The carbonization of walnut shell under water vapor at 800 °C increased the oxidation resistance of supported magnetic particles. Second step of TGA profiles indicated the weight loss of AC@Fe_3O_4-NH_2-COOH with increasing temperature from 250 to 400 °C, while decomposition of AC@Fe_3O_4 was in the range of 250-300 °C, approximately. There was a significant weight loss in the second step which might be attributed to existence of amino acids groups over supported magnetic nanoparticles.

As seen in Fig. 2, the diffraction structures of as-prepared AC@Fe_3O_4 and AC@Fe_3O_4-NH_2-COOH were determined by XRD.

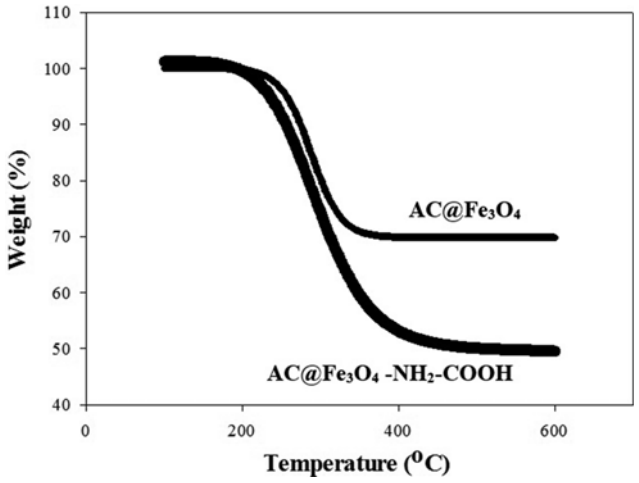

Fig. 1. TGA experiments for AC@Fe_3O_4 and AC@Fe_3O_4-NH_2-COOH, at 1,000 °C and initial weight of sample=10 g.

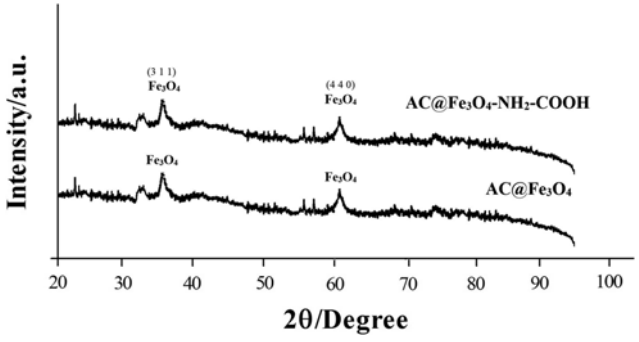

Fig. 2. XRD results for AC@Fe_3O_4-NH_2-COOH and AC@Fe_3O_4.

The patterns show the characteristic peaks for Fe_3O_4 at 2θ= (35.42°, ICDD=00-001-1111 and 62.260°, ICDD=00-003-0862) by X'PertHighScore software version 1.0d produced by PANalytical BV Almelo, the Netherlands.

According XRD patterns, Fe_2O_3 (hematite) and FeO crystallites, which must be generated peak at 2θ=33.28°, 42.19°, respectively, were not detected over magnetic nanoparticles including AC@Fe_3O_4 and AC@Fe_3O_4-NH_2-COOH. These results indicate that the surface coating of NH_2-COOH did not alter the phase of the Fe_3O_4 cores over prepared activated carbon. Walnut shell activated carbon prepared by physical activation had insignificant crystallinity and an amorphous phase could be detected from Fig. 2. Fe_3O_4 crystallites were generated over walnut activated carbon during co-precipitation method. The intensity of diffraction peaks at the similar degree decreased with adding oxygen functional groups on AC@Fe_3O_4. The Fe_3O_4 peaks in the XRD profiles had wider line

Table 1. Boehm analysis results of AC@Fe_3O_4 and AC@Fe_3O_4-NH_2-COOH (mequiv/g)

Raw material	Basic groups	Lactonic groups	Carboxylic groups	Phenolic groups	Total acidic groups= Total oxygen groups
AC@Fe_3O_4	0.45	0.42	0.35	0.30	1.07
AC@Fe_3O_4 -NH_2-COOH	0.45	0.46	0.53	0.49	1.48

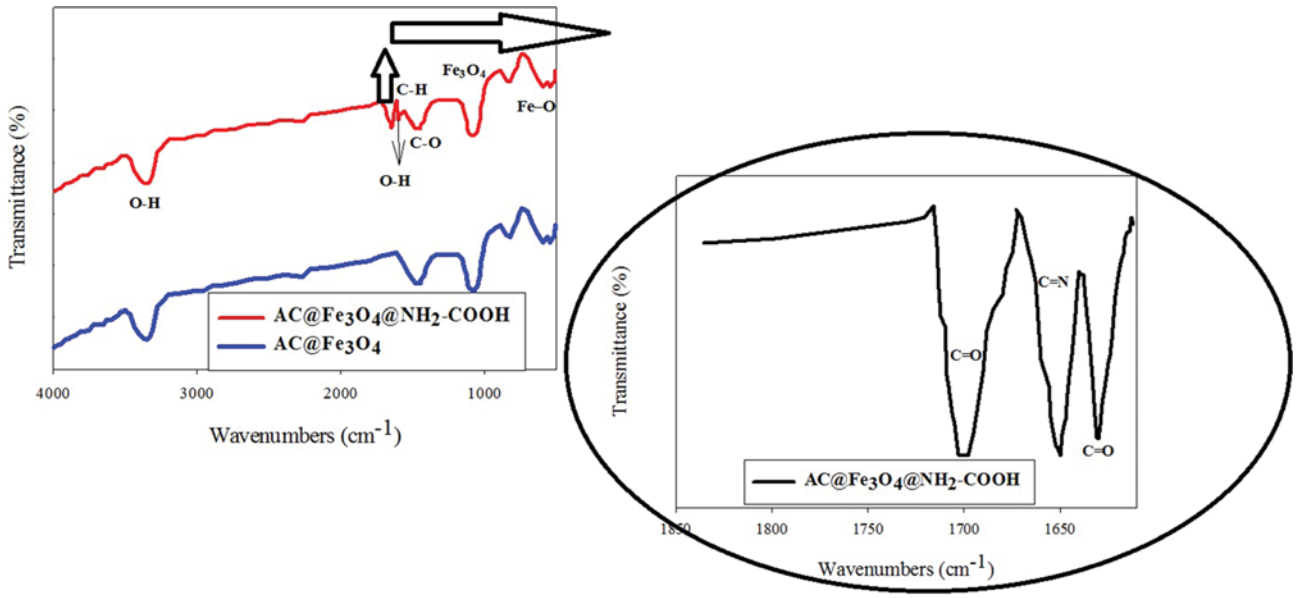

Fig. 3. FT-IR results for AC@Fe_3O_4 and AC@Fe_3O_4-NH_2-COOH and AC@Fe_3O_4.

broadening, indicating that the co-precipitation method and activated carbon as a support can provide smaller well-dispersed particles. The crystallite sizes with spheres shapes were calculated by Scherrer equation [15] given by Eq. (2):

$$D = \frac{K\lambda}{\beta \cos\theta} \quad (2)$$

where D is the mean crystallite diameter (nm), K is the dimensionless shape factor (spheres=0.89), λ is the X-ray wavelength (X-ray tube: Cu, λ=0.154 nm), β is the line broadening at half the maximum intensity and θ is the Bragg angle. The results indicate that the size of iron crystallites formed on carbonaceous support was less than 30 nm.

FT-IR graphs of pure AC@Fe_3O_4, and AC@Fe_3O_4@ NH_2-COOH nanoparticles from 500-4,000 cm^{-1} are shown in Fig. 3. FT-IR patterns represent significant absorption bands at around 578.51 and 585 cm^{-1}, which corresponds to Fe-O vibration related to Fe_3O_4 [26,27]. Broad bands at around 1,096 cm^{-1} correspond to the Fe_3O_4 particles for both samples. Similar results were also reported by Xu et al. [27], who found that the peaks at 1,096.19 cm^{-1} represent the magnetic particles. Generated peaks at about 1,400 to 1,570 cm^{-1} demonstrated C-O stretch and bending of NH_2 in AC@Fe_3O_4@ NH_2-COOH [28,29], respectively. In addition, the vibration of C-H might be observed close to the 1,487 cm^{-1} which also was offered by Wang [28]. Three new peaks appeared over the cure of AC@Fe_3O_4@ NH_2-COOH from 1,630 to 1,700 cm^{-1}. The characteristic peaks at about 1,630 cm^{-1} and 1,700 cm^{-1} are due to the C=O (stretch) which can confirm the preparation method to functionalize the supported magnetic particles with amino groups, and another peak at 1,650 cm^{-1} illustrates C=N bond [27-30]. O-H bond is observed at two peaks (3,350 and 1,600 cm^{-1}) over both Ft-IR curves. FT-IR results revealed that supported magnetic particles have been functionalized with COOH and NH_2 groups during preparation method.

The TEM results and particle size distribution of single activated carbon, Fe_3O_4 and the amino-functionalized magnetic nanoparticles (AC@ Fe_3O_4, AC@Fe_3O_4-NH_2-COOH) supported on walnut shell activated carbon are seen in Figs. 4(a) and 4(b), respectively. It was determined from these micrographs that dark dots represented Fe_3O_4 crystallites, which was confirmed by XRD analysis. The average Fe_3O_4 crystallites sizes were measured by Clemex software to be between 5 to 50 nm over walnut activated carbon. The results also established that prepared magnetic adsorbent with high dispersion was formed over walnut activated carbon, which also confirmed Scherrer equation results and highlighted the role of activated carbon as a support. Comparison between samples was notable that the amino-functionalization did not significantly affect the particle agglomeration.

The architectural porosity of AC@Fe_3O_4-NH_2-COOH was analyzed by N_2 adsorption-desorption test, which indicates type-IV isotherm that is typical for mesoporous adsorbent shown in Fig. 5. Important feature of type IV isotherms is the presence of micropores associated with mesopores. The surface area for the AC@Fe_3O_4-NH_2-COOH was calculated 450 m^2/g and 448.21 m^2/g by BET and t-plot theories, respectively, while the surface area of walnut activated carbon was measured as 840 m^2/g by BET theory [15]. It is shown the surface area decreased by forming Fe_3O_4 on the activated carbon, which is confirming the XRD Results. However, the activated carbon as hydrophobic adsorbent has supplied porous media for forming magnetic nanoparticles. Adding carboxylic groups to the magnetic nanoparticles has no considerable effect on the surface morphology and surface area of AC@Fe_3O_4 while the calculated area was 455 m^2/g.

XRF analysis was applied to illustrate the chemical elements of AC@Fe_3O_4-NH_2-COOH and the amount of Fe_3O_4 was coated on walnut shell-activated carbon. Reported results in Table 2 indicate that the prepared supported magnetic adsorbent has the same amount of carbon and Fe, which is in the good agreement with

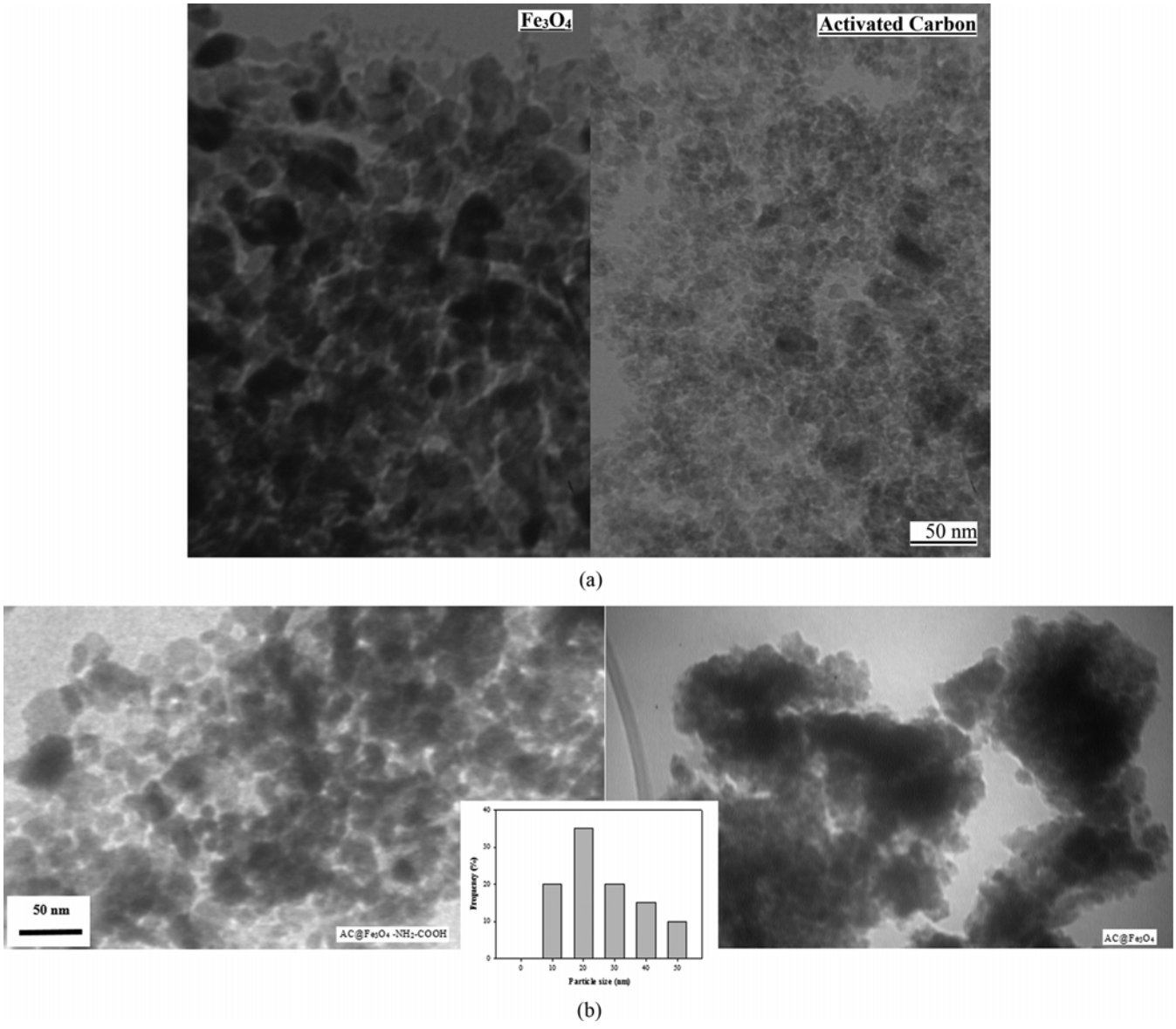

Fig. 4. (a) TEM results for walnut shell-activated carbon and Fe_3O_4, (b) TEM results for AC@Fe_3O_4-NH_2-COOH and AC@Fe_3O_4.

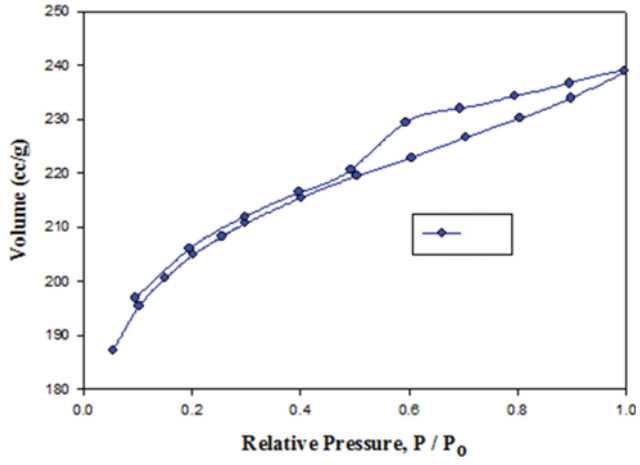

Fig. 5. N_2 adsorption-desorption of AC@Fe_3O_4-NH_2-COOH.

Table 2. XRF results for AC@Fe_3O_4-NH_2-COOH.

Chemical element wt%	C	Fe	O	Other element
AC@Fe_3O_4@SiO_2-NH_2-COOH	36.02	35.28	19.45	9.25

the scopes of the preparation method to achieve Activated-Carbon: Fe_3O_4 weight ratios of 1 : 1.

2. Selection of the Best Back Propagation Training Algorithm

The best appropriate backpropagation (BP) training algorithm was selected from nine training algorithms. To achieve this target, a comparison was made between all those algorithms. For all feed forward (FF) algorithms, a three-layer ANN with a tangent sigmoid transfer function (tansig) at hidden layer and a linear transfer function (purelin) at output layer were used. Fig. 6 shows the ANN structure and the flowchart which was used to predict the adsorp-

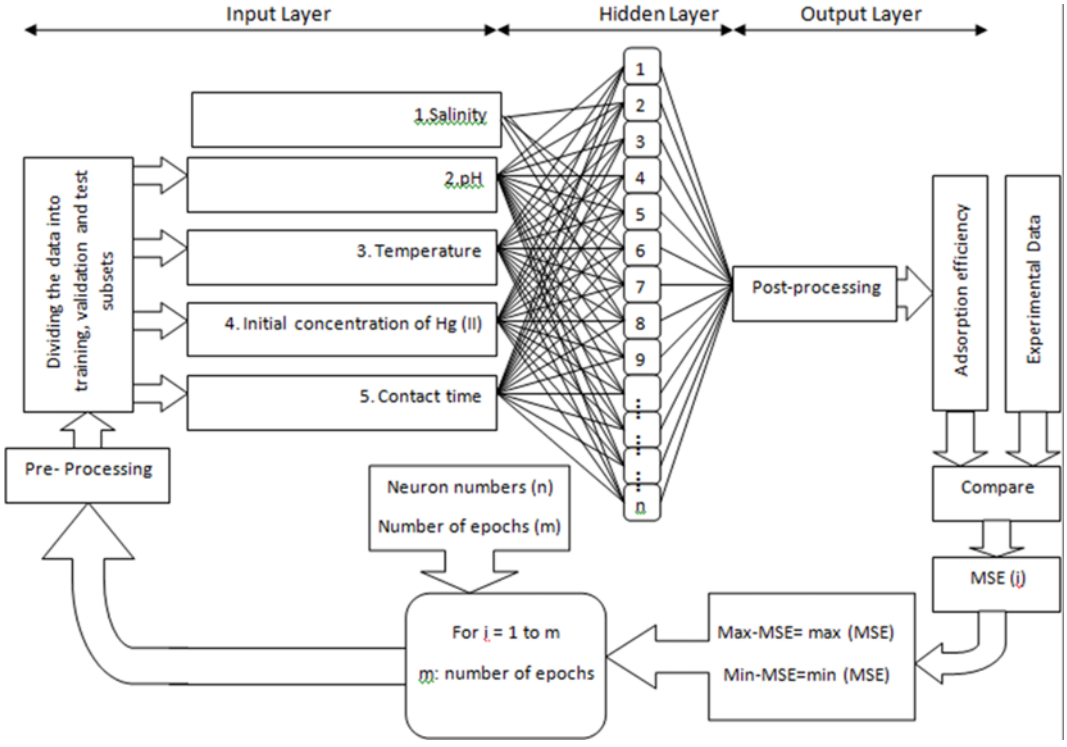

Fig. 6. ANN structure and related flowchart used in this study.

Table 3. MSE values for different BP training algorithms with different neuron numbers for AC@Fe_3O_4-NH_2-COOH

Neuron number in second layer	Trainrp	Traincgf	Traincgp	Traincgb	Trainlm	Trainscg	Trainbfg	Trainoss
1	0.0591	0.0591	0.0591	0.0591	0.0591	0.0591	0.0591	0.0591
2	0.0157	0.0177	0.0094	0.0076	0.0059	0.0104	0.0095	0.0099
3	0.0086	0.0101	0.0048	0.0075	0.0021	0.0072	0.0052	0.0099
4	0.0039	0.0074	0.0062	0.0064	0.001	0.004	0.0039	0.0064
5	0.0056	0.0056	0.0043	0.0048	0.0007	0.0063	0.0032	0.0041
6	0.0041	0.0061	0.0044	0.0041	0.0002	0.0042	0.0036	0.0055
7	0.0037	0.0023	0.003	0.0037	0	0.0038	0.0025	0.0036
8	0.0022	0.0026	0.0028	0.0034	0	0.0048	0.0023	0.0044
9	0.0035	0.002	0.0031	0.0017	0	0.0023	0.0015	0.0035
10	0.002	0.0022	0.0026	0.0022	0	0.002	0.0014	0.0019
11	0.0032	0.0028	0.0009	0.002	0	0.0014	0.0009	0.0018
12	0.0022	0.0023	0.0013	0.0021	0	0.0024	0.0016	0.0029
13	0.002	0.0009	0.0012	0.0016	0	0.0017	0.0016	0.0024
14	0.0023	0.0017	0.0015	0.0013	0	0.0019	0.0014	0.0023
15	0.0025	0.0009	0.0013	0.0017	0	0.0014	0.0011	0.0025
16	0.0007	0.0025	0.0022	0.0014	0	0.0012	0.0005	0.0035
17	0.0018	0.001	0.0013	0.0019	0	0.0018	0.0009	0.0012
18	0.001	0.0009	0.001	0.0016	0	0.0014	0.0006	0.0011
19	0.0015	0.0016	0.001	0.0011	0	0.0012	0.0002	0.0012
20	0.0014	0.0019	0.0009	0.0011	0	0.0007	0.0006	0.0019

tion efficiency in this study. To determine the best algorithm, all algorithms were evaluated with different neuron numbers from 1 to 20 neurons. Table 3 shows a comparison among different back propagation (BP) training algorithms and the minimum MSE (Eq. (3) [18]) values from calculation of 200 epochs for AC@Fe_3O_4-NH_2-COOH. The results show that LMA is the best suited BP training algorithm for supported magnetic nanoparticles, and it results in smaller MSE for almost all neuron numbers. As shown in these

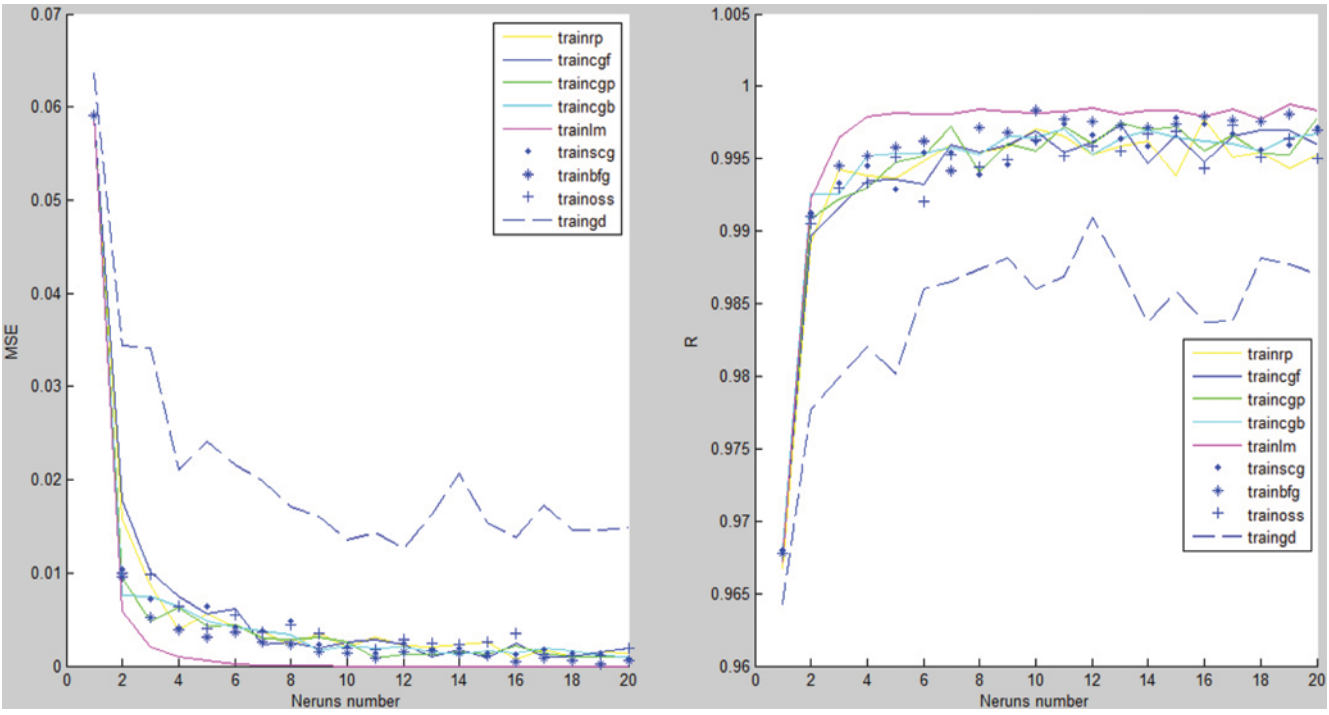

Fig. 7. Maximum MSE and R^2 values for different neurons number for AC@Fe_3O_4-NH_2-COOH.

tables, the MSE is suddenly reduced to about 3.3898E-24 at eight neurons and upper for AC@Fe_3O_4-NH_2-COOH which can be assumed zero, but for other algorithms there is not much reduction in the MSE values by increasing neuron numbers.

$$MSE=\frac{1}{N}\sum_{p=1}^{N}e_p^2=\frac{1}{N}\sum_{p=1}^{N}(t_p-O_p)^2 \quad (3)$$

where N=number of the patterns; p=index number for pattern; t_p=target value for the p^{th} pattern; o_p=output of the p^{th} pattern; and e_p=difference between t_p and o_p.

3. Optimum Neuron Number for LMA

To determine optimal neuron number for LM training algorithm and other training algorithms, the MSE value for each neuron number was calculated for 200 epochs and the maximum MSE was selected to compare with other neurons number. Fig. 7 shows the results of MSE and R^2 versus neuron number for AC@Fe_3O_4-NH_2-COOH for different BP training algorithms. Maximum amount of MSE for AC@Fe_3O_4-NH_2-COOH with eight neurons is about zero 0.0293, 0.0209 and 0.0338, respectively. Consequently, the optimum neuron number for AC@Fe_3O_4-NH_2-COOH would be eight, which corresponds to minimum values of MSE on the following figures.

To investigate the agreement between ANN outputs (predicted) and experimental data (targets), regression analysis was performed for AC@Fe_3O_4-NH_2-COOH, which are shown in Fig. 8. The agreement is satisfactory and the best linear fits are solid red lines with correlation coefficients of 0.9984 for AC@Fe_3O_4-NH_2-COOH.

4. Sensitivity Analysis

To evaluate the effect of each parameter, a sensitivity analysis was performed. The effectiveness of each parameter and combination of two, three, four and five of them was evaluated by the optimal ANN structure using LMA with eight neuron numbers for AC@Fe_3O_4-NH_2-COOH. Input parameters were temperature, initial concentration, time, salinity and pH. Table 4 shows results of sensitivity analysis for different combinations of variables. As seen, pH and salinity is the most effective parameter among one-variable group. The minimum value of MSE is for combination of (time and pH) among two variable group; the combination of (salinity+pH+time) has the minimum value of MSE in three parameter

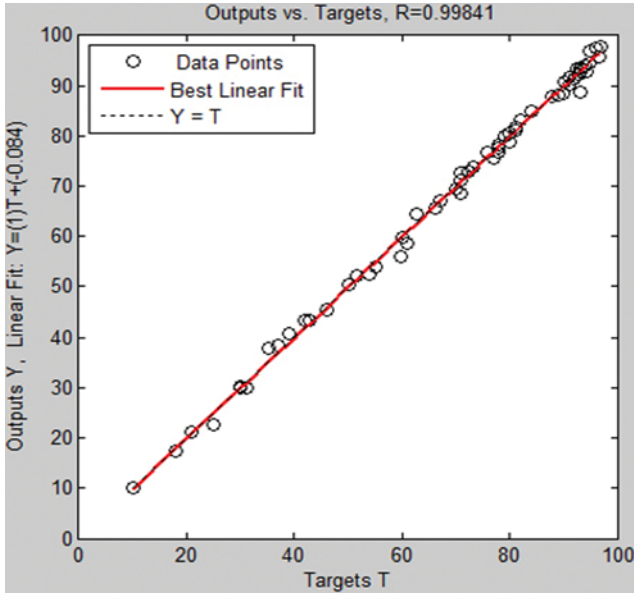

Fig. 8. The ANN output (predicted) plotted versus corresponding targets for AC@Fe_3O_4-NH_2-COOH.

Table 4. Results of sensitivity analysis for AC@Fe_3O_4-NH_2-COOH

Operating parameters	MSE	R^2	Epoch	BLE
Salinity	527.0089	0.1962	4	Y=0.071x+67
Time	363.2152	0.5703	6	Y=0.27x+53
pH	257.3455	0.7212	4	Y=0.54x+31
Temp.	514.9419	0.23379	3	Y=0.056x+62
Initial conc.	505.8889	0.2186	4	Y=0.049x+65
Salinity+Time	335.8622	0.61168	9	Y=0.43x+39
Salinity+pH	259.3600	0.71489	8	Y=0.5x+36
Salinity+Temp.	494.7416	0.27426	7	Y=0.1x+62
Salinity+Initial conc.	498.2715	0.28873	7	Y=0.13x+62
Time+pH	68.0245	0.9339	6	Y=0.85x+11
Time+Temp.	327.6018	0.6237	10	Y=0.37x+42
Time+Initial conc.	330.9249	0.6131	10	Y=0.36x+45
pH+Initial conc.	222.2313	0.76506	6	Y=0.63x+25
pH+Temp.	252.8869	0.7233	6	Y=0.54x+32
Temp.+Initial conc.	487.0759	0.29049	6	Y=0.1x+64
Salinity+pH+Time	53.9753	0.9485	9	Y=0.92x+6.7
Salinity+pH+Initial conc.	207.7535	0.7800	10	Y=0.62x+26
Salinity+pH+Temp.	247.7276	0.7488	12	Y=0.52x+36
Salinity+Time+pH+Temp.	35.1547	0.96658	18	Y=0.96x+3.4
Salinity+Time+pH+Initial conc.	37.2642	0.9655	11	Y=0.92x+6.9
Total parameters	3.3898E-24	0.9984	24	Y=x+0.084

group, and finally the combination of (salinity+pH+time+temperature) has the minimum value of MSE in four parameter group. Generally, it is obvious from Table 4 that by enhancement of the number of parameters the value of MSE decreases.

5. Mercury Ions Adsorption

5-1. Effect of pH and Salinity on Hg (II) Removal

Mercury ion adsorption on AC@Fe_3O_4-NH_2-COOH as a function of pH suspension (2-11) and variant concentrations of NaCl (1,000-30,000 ppm) is shown in Fig. 9(a). It is obvious that pH can be an effective parameter on adsorption of mercury ions in the presence of salinity in the aqueous solutions [4,5]. As a finding from Fig. 9(a), removal efficiency of mercury ions increases sharply with increasing pH from 2 to 7 for any salinity concentrations. Significant role of pH appeared from value of 7, while there is negligible difference between removal efficiency of mercury at different NaCl concentrations. In contrast, removal efficiency of Hg (II) ions increases mildly from pH 7 to 11. Therefore, mercury ions sorption in basic solutions over supported magnetic nanoparticles on walnut activated carbon in the presence of oxygen functional groups can be the efficient and feasible methods. Mercury ions in the synthesized solutions are generally positive charge during adsorption process. Also, the charge of supported magnetic nanoparticle is positive below the pH of 7. Therefore, there is one competition between mercury ions, H^+ and Na^+ ions present in solution for sitting on the surface of adsorbent. The electrostatic attraction between the OH^- ions and positive ions of mercury in the solution at pH>7 and also the attraction between the surface of supported magnetic nanoparticles with positive charge and OH^- ions can increase the removal efficiency of mercury ions and decrease the significant effect of salinity. In addition, $Hg(OH)_2$ formation may play an important role for covering the effect of salinity at high alkaline pH solutions. As shown in Fig. 9(b), good agreement between estimated artificial neural network model and the experimental data can be observed clearly.

5-2. Effect of Temperature

Adsorption of mercury ions was measured a function of temperature and time contact over prepared magnetic nanoparticles in the different temperatures in the range of 25-45 °C under constant operating condition containing, adsorbent dosage of 0.05 g, pH of 7, stirrer velocity of 600 rpm, salinity of 25,000 ppm and initial concentration of 50 ppm. As mentioned, no significant effect of salinity was observed at pH as high as 7; therefore, a pH value of 7 was selected as an optimum and constant operating parameters for studying the effect of other important parameters. The experimental data indicate that removal efficiency of mercury ions increases with increasing in the temperature of solutions, displaying an endothermic nature of adsorption phenomena. As shown in Fig. 10(a), mercury ion uptake onto AC@Fe_3O_4-NH_2-COOH was just dependent on the contact time while reaching equilibrium contact time, which was about 60 min. Generally, the removal efficiency of mercuric ion adsorption enhances sharply with contact time in initial stages (0-30 min) as seen in Fig. 10(a). This is due to the attractive forces between mercuric ions and fresh active sites over surface area of magnetic adsorbent while there are many fresh sites for occupying by mercury ions during initial stages. Adsorption can be described by several steps, including external diffusion (migration of the ions from the solution to the interface of liquid phase), migration of ions to the surface of adsorbent and internal diffusion (migration of ions from external surface to the internal surface containing pores). Therefore, diffusion is the rate

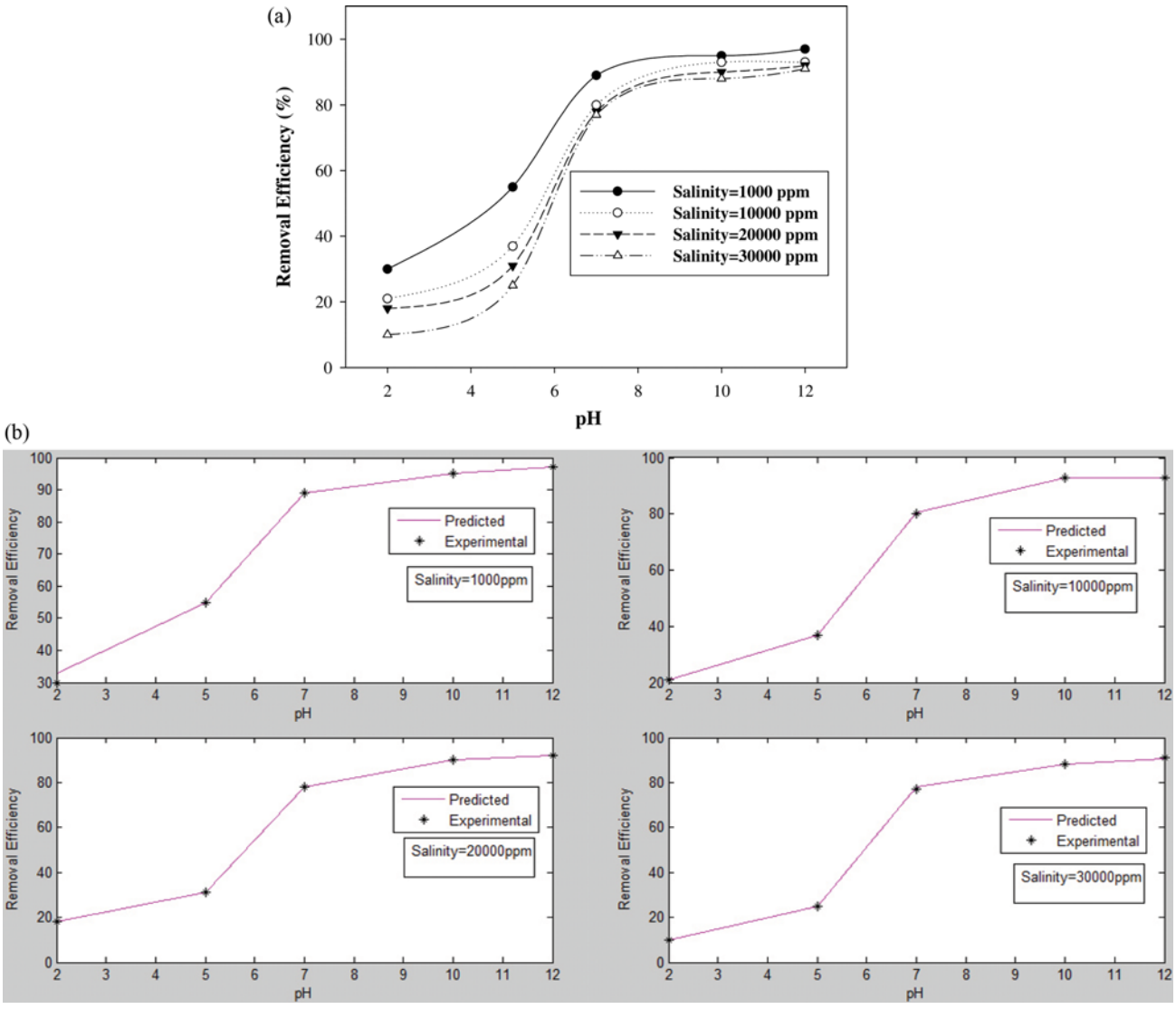

Fig. 9. (a) Effect of pH and Salinity on the adsorption of Hg (II), (b) agreement between ANN predictions and experimental data as a function of pH for AC@Fe_3O_4-NH_2-COOH.

determining step of an adsorption in this studied range of temperature for removal of mercury ions, which increases with increasing temperature of solution. Similar results were offered in the literature review [2] that the beneficial adsorption of heavy metal ions was at high temperatures. As seen in Fig. 10(b), there is a good compromise between experimental and ANN model results for prediction of the adsorption process.

5-3. Effect of Hg (II) Initial Concentration

Initial concentration of mercury ions in solutions is a significant parameter for describing the adsorption of mercuric ions in the presence of salinity. Several batch experiments were implemented with different concentrations in the range of 10-80 ppm versus contact time under constant conditions containing, a fixed temperature of 25 °C, NaCl concentration of 25,000 ppm, pH of 7 and adsorbent dosage of 0.05 g. Based on the open literature review, the removal of mercury ions from aqueous solutions enhances by increasing the initial concentration of ions due to have the greater driving force of adsorption. In addition, mercury ion adsorption increased sharply in the initial contact times in the range of 0-20 min, afterward adsorption reached equilibrium in about 60 min for all various initial concentration mercury ions as seen in breakthrough curves of Fig. 11(a). As mentioned, there is no significant salinity effect in pH higher value of 7. Output of neural network model and experimental data indicated the effect of initial concentration of mercury ions, plotted in Fig. 11(b). Prediction model is in a good estimation with experimental data as plotted in Fig. 11(b). It is notable that similar consequences were achieved by increasing initial concentrations of mercury ions with other non-magnetic and magnetic adsorbents. In our previous study, we reported more active sites in low initial concentration due to adsorb ions sharply in the beginning stages. Zabihi et al. [2] also published that the percentage of mercury ion removal was dependent on change of the initial concentration of mercury ions in aqueous solutions. Similar results also were achieved by Alijani et al. [31],

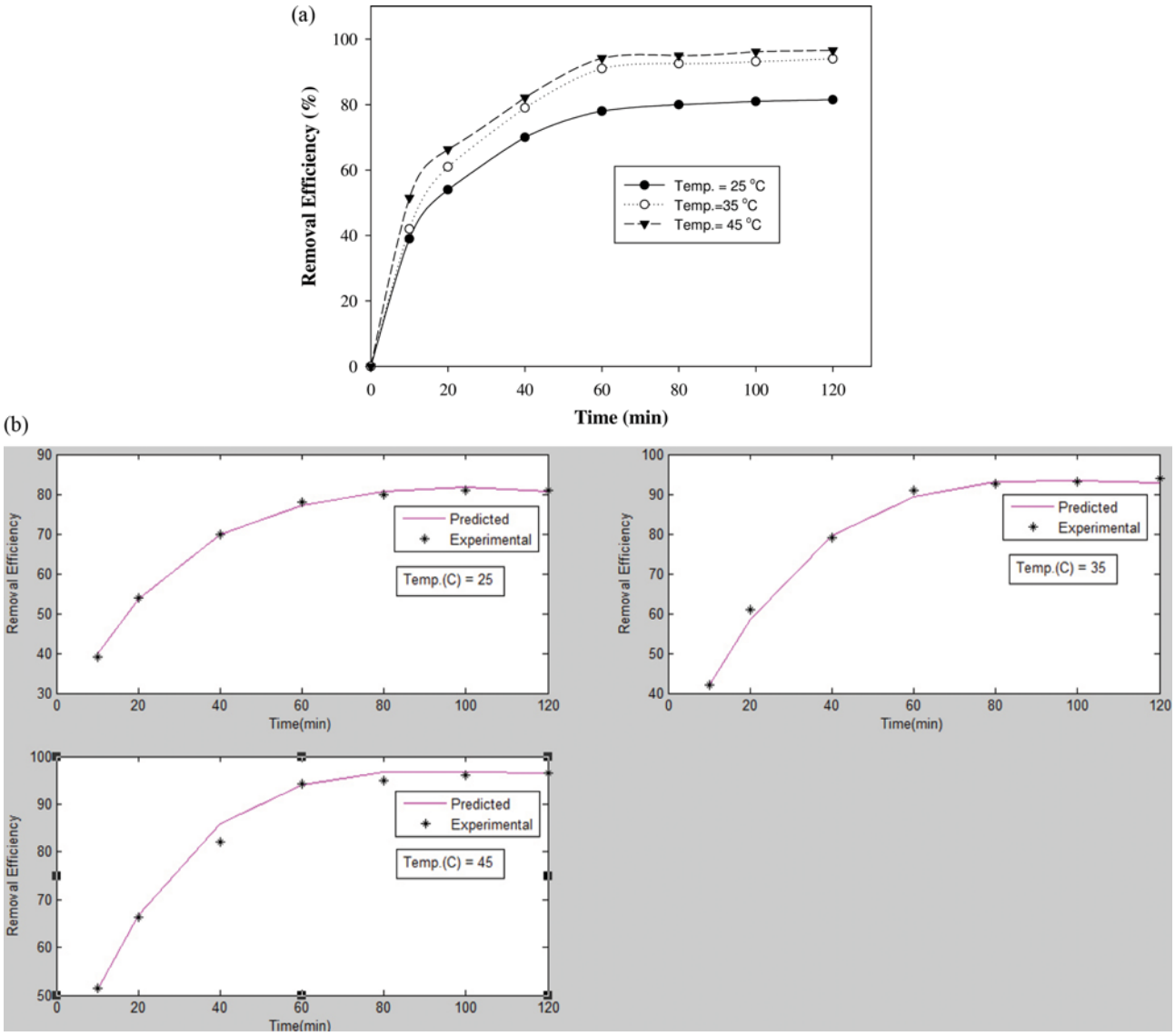

Fig. 10. (a) Effect of temperature on the adsorption of Hg (II), (b) agreement between ANN predictions and experimental data as a function of temperature for AC@Fe_3O_4-NH_2-COOH.

who found that the adsorption process reached equilibrium in about 60 min for all batch experiments during aging solutions. Magnetic nanoparticles adsorbents also were investigated for removal of heavy metal ions from aqueous solutions, recently. Liu and co-workers [5] carried out experiments for removal of copper ions from saline aqueous solutions by applying magnetic nanoparticles-EDTA in operating conditions similar to this present study. It was found that adsorption capacity of copper ions increased by increasing initial concentrations in from 1 to 6 ppm.

Maximum adsorption capacity of prepared magnetic adsorbent was calculated by Langmuir isotherm. Constant parameters of Langmuir model were determined under operating condition, including various initial concentration of mercury ions (10, 30, 50 and 80 ppm), a fixed dosage of adsorbent (0.0165 g) per 0.05 liter solution at a constant temperature (25 °C) while keeping all other parameters constant. All experiments were carried out for 12 hours to reach the equilibrium concentration of Hg (II). Obtained data was fitted by linearized Langmuir model given by [3]:

$$\frac{C_e}{q_e} = \frac{1}{q_m b} + \frac{1}{q_m} C_e \tag{4}$$

where q_m (mg/g) is the amount of adsorption of mercuric ions and b (*l*/mg) is the Langmuir constant related to the energy of adsorption. The amount of Hg (II) adsorption was measured by [2]:

$$q_e = \frac{(C_0 - C_e)V}{W} \tag{5}$$

where q_e (mg/g) is the amount of adsorbed mercury ions over adsorbent, C_0 and C_e (ppm) are the initial and equilibrium concentration of mercury ions in the solution, V is the solution volume (*l*) and W is the dosage of adsorbent (g). Correlation coefficient of R^2=0.9946 shows the strongest relationship between Langmuir

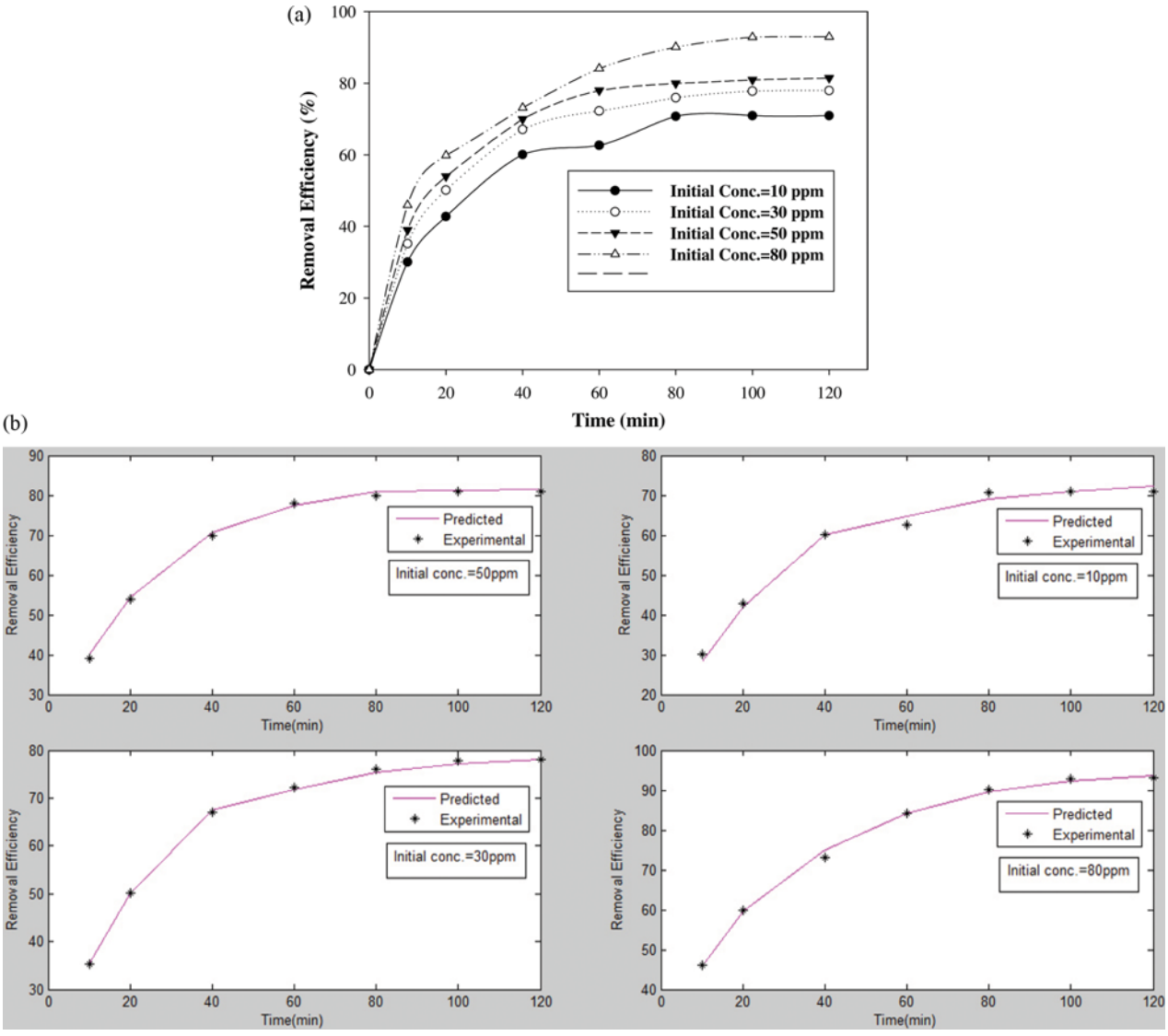

Fig. 11. (a) Effect of initial concentration of mercury on the adsorption of Hg (II), (b) agreement between ANN predictions and experimental data as a function of initial concentration of Hg(II) for AC@Fe_3O_4-NH_2-COOH.

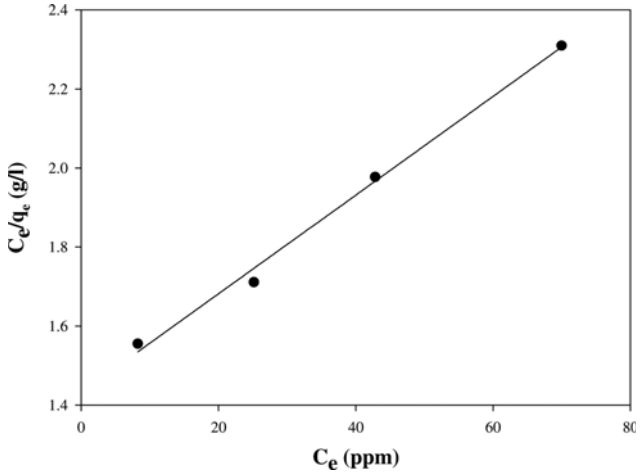

Fig. 12. Langmuir plot for adsorption of mercury ions at a constant temperature (25 °C).

equation and experimental data (Fig. 12). The values of amount of adsorbed mercury ions and b constant were 80 (mg/g) and 0.0088 (*l*/mg), respectively. Adsorbed equilibrium amount of mercury ions on the novel magnetic adsorbent after 12 hours was 5.3030, 14.6970, 21.6667 and 30.3030 mg/g, respectively. Consequence adsorption capacity in this present study for example is larger than Malt spent rootlets (50.4 mg/g) [32] with no exist of NaCl ions in solutions.

6. Kinetic Study

Kinetic study of mercury adsorption on the prepared magnetic nanoparticles was also investigated by applying the pseudo-first and second-order rate equations.

To study the kinetic of mercury ion surface adsorption, adsorption capacity of the magnetic adsorbent was calculated at various temperatures (25-45 °C) during time. Afterwards, the integrated form of the pseudo-first and second-order was studied, which are given by [3]:

(Pseudo-first-order) (6)

$$q_t = \frac{t}{(1/K_2 q_e^2) + (t/q_e)} \quad \text{(Pseudo-second-order)} \tag{7}$$

where q_t (mg/g) is the amount of adsorbed mercury ion on the magnetic adsorbent at time t, q_e is the equilibrium sorption uptake at time t=∞, and K_1 (min^{-1}) and K_2 (gm g^{-1} min^{-1}) are the rate constants of first and second-order adsorption, respectively.

The values of constant parameters were directly determined by the linear regression. The fitted curves of the kinetic models along with the experimental data at three different temperatures and constant initial concentration of 50 ppm are seen in Figs. 13 and 14. The constant rate values and the corresponding correlation coefficients summarized in Table 5 are in good agreement with experimental data. Obtained results suggest that the adsorption of mercury ions follows the second-order kinetic equation.

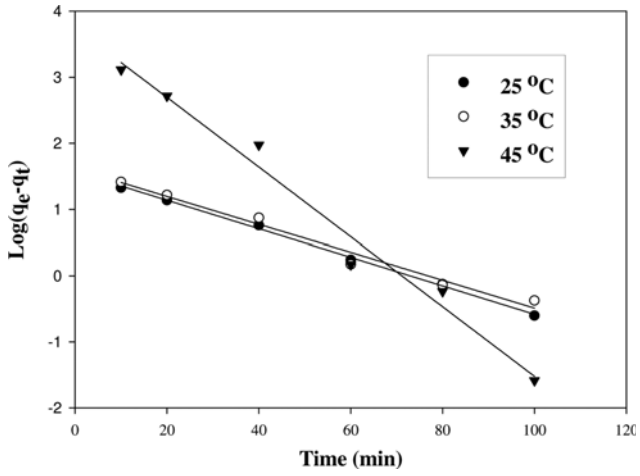

Fig. 13. Regression plots for the adsorption of Hg (II) at 25, 35, and 45 °C, first-order model.

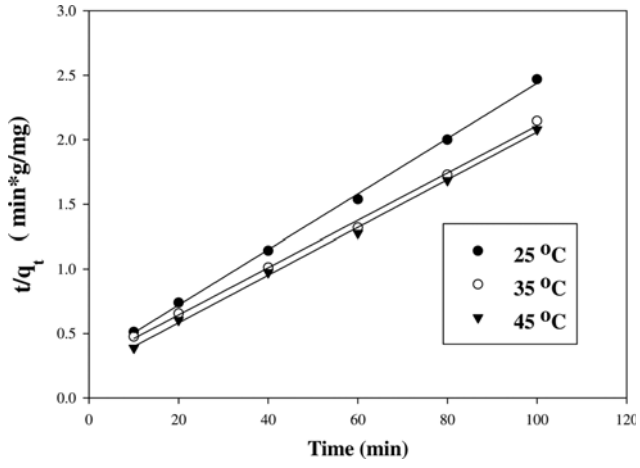

Fig. 14. Regression plots for the adsorption of Hg (II) at 25, 35, and 45 °C, second-order model.

Table 5. The constant parameters of the kinetic models for adsorption of Hg(II)

Kinetic model	Fitted parameters K_1 (min^{-1}), K_2 (gm g^{-1} min^{-11})	R^2	Temp. (°C)
Pseudo-first-order	K_1=0.0495	0.9979	25
Pseudo-first-order	K_1=0.0485	0.9780	35
Pseudo-first-order	K_1=0.1214	0.9794	45
Pseudo-second-order	K_2=0.0738	0.9988	25
Pseudo-second-order	K_2=0.0661	0.9973	35
Pseudo-second-order	K_2=0.0861	0.9982	45

CONCLUSIONS

Adsorption of Hg (II) on the prepared supported magnetic nanoparticles was investigated in the presence of NaCl in the solutions. Magnetic Fe_3O_4 nanoparticles were formed on the activated carbon derived from walnut shell, by co-precipitation method. Addition of oxygen functional containing NH_2-COOH groups increased the capacity of adsorbent for removal of mercuric ions from saline aqueous solutions. To the best of our knowledge there is no report in the open literature review on synthesizing the supported magnetic nanoparticles over walnut shell activated. Study of salinity effect of solutions indicated that salinity plays no significant role in the adsorption of mercury ions at pH value in range of 7-11. Maximum adsorption capacity of mercury was calculated 80 mg/g by Langmuir equation, while the salinity of solutions was 25,000 ppm. Results also indicated that pseudo-second-order model can justify the kinetic behavior of mercury adsorption. Removal efficiency of mercury ions increased with both increasing temperature of solutions and initial concentrations of mercury ions. A three layer back-propagation neural network with tangent sigmoid transfer function (tansig) at hidden layer, and a linear transfer function (purelin) at output was coded to predict and simulate the Hg(II) ions removal from saline aqueous solution by AC@Fe_3O_4-NH_2-COOH. According to the calculated MSEs, the Levenberg-Marquardt algorithm (LMA) was the best training algorithm among nine BP algorithms for AC@Fe_3O_4-NH_2-COOH while the optimum neurons number was eight. The sensitivity analysis showed that by increasing the number of parameters the value of MSE decreases. It was found that pH and salinity are the most effective parameters. In summary, ANN results showed that the proposed model could effectively predict the process of adsorption.

ACKNOWLEDGEMENT

The authors are greatly thankful to the assistance of Institute of Materials and Energy, Iran.

NOMENCLATURE

C_0 : initial metal ion concentration (Eq. (1), (5))
C_e : equilibrium concentration (Eq. (1), (4), (5))
V : volume of the solution (Eq. (5))
W : weight of sorbent (Eq. (5))
q_e : equilibrium amount adsorbed (Eq. (4), (5), (6), (7))
q_m : Langmuir constant related to the maximum adsorption capacity (Eq. (4))
b : Langmuir constant related to the energy or net enthalpy of adsorption (Eq. (4))

q_t : amount adsorbed at time t (Eq. (6), (7))
K_1 : rate constant of first-order adsorption (Eq. (6))
K_2 : rate constant of the second-order adsorption (Eq. (7))
t : adsorption time (Eq. (6), (7))

REFERENCES

1. K. Johari, N. Saman, S. Tien Song, C. S. Chin, H. Kong and H. Mat, *International Bio-deterioration Biodegradation*, **109**, 45 (2016).
2. M. Zabihi, A. Haghighi-Asl and A. Ahmadpour, *J. Hazard. Mater.*, **174**, 251 (2010).
3. M. Zabihi, A. Ahmadpour and A. Haghighi-Asl, *J. Hazard. Mater.*, **167**, 230 (2009).
4. X. Zhang, Y. Wang and S. Yang, *Polymers*, **114**, 521 (2014).
5. Y. Liu, M. Chen and Y. Hao, *Chem. Eng. J.*, **218**, 46 (2013).
6. Y. Wang, Q. Wei and Y. Huang, *Mater. Lett.*, **157**, 67 (2015).
7. A. Wasti and M. A. Awan, *J. of the Association of Arab Universities for Basic and Applied Sciences*, **20**, 26 (2016).
8. B. N. Papas and J. L. Whitten, *Surface Sci.*, **651**, 22 (2016).
9. E. L. Uzunova and H. Mikosch, *Micropor. Mesopor. Mater.*, **232**, 119 (2016).
10. N. H. Mthombeni, S. Mbakop, A. Ochieng and M. S. Onyango, *J. Taiwan Inst. Chem. Engineers*, 9 (2016).
11. S. Andrejkovičová, A. Sudagar, J. Rocha, C. Patinha, W. Hajjaji, E. Ferreira da Silva, A. Velosa and F. Rocha, *Appl. Clay Sci.*, **126**, 141 (2016).
12. M. G. Moritz and M. Moritz, *Mater. Sci. Eng.*, **69**, 815 (2016).
13. V. Russo, D. Masiello, M. Trifuoggi, M. D. Serio and R. Tesser, *Chem. Eng. J.*, **302**, 287 (2016).
14. N. Srivastava, A. K. Thakur and V. K. Shahi, *Carbohydr. Polym.*, **136**, 1315 (2016).
15. M. Zabihi, F. Khorasheh and J. Shayegan, *RSC Adv.*, **5**, 5107 (2015).
16. S. Nethaji, A. Sivasamy and A. B. Mandal, *Bioresour. Technol.*, **134**, 94 (2013).
17. J. H. Xu, N. Y. Gao, D. Y. Zhao, D. Yin, H. Zhang, Y. Gao and W. Shi, *Sep. Purif. Technol.*, **147**, 9 (2015).
18. K. Yetilmezsoy and S. Demirel, *J. Hazard. Mater.*, **153**, 1288 (2008).
19. S. Agarwal, I. Tyagi, V. Kumar Gupta, M. Ghaedi, M. Masoomzade, A. M. Ghaedi and B. Mirtamizdoust, *J. Mol. Liq.*, **218**, 354 (2016).
20. R. Khandanloua, H. R. Fard-Masoumi, M. B. Ahmad, K. Shameli, M. Basri and K. Kalantari, *Ecological Engineering*, **91**, 249 (2016).
21. I. Dimopoulos, J. A. Chronopoulos-Serelia and S. Lek, *Ecol. Model.*, **120**, 157 (1999).
22. S. Aber, N. Daneshvar, S. M. Soroureddin, A. Chabok and K. Asadpour-Zeynali, *Desalination*, **211**, 87 (2007).
23. N. Daneshvar, A. R. Khataee and N. Djafarzadeh, *J. Hazard. Mater.*, **B137**, 1788 (2006).
24. M. H. Fatehi, J. Shayegan, M. Zabihi and I. Goodarznia, *J. Environ. Chem. Eng.*, **5**, 1754 (2017).
25. H. Hasar, *J. Hazard. Mater.*, **B97**, 49 (2003).
26. S. Bao, L. Tang, K. Li, P. Ning, J. Peng, H. Guo, T. Zhua and Y. Liu, *J. Colloid Interface Sci.*, **462**, 235 (2016).
27. Y. Xu, Q. Dang, C. Liu, J. Yan, B. Fan, J. Cai and J. Li, *Colloids Surf., A: Physicochem. Eng. Aspects*, **482**, 353 (2015).
28. S. Wang, K. Wang, C. Dai, H. Shi and J. Li, *Chem. Eng. J.*, **262**, 897 (2015).
29. S. H. Huang and D. H. Chen, *J. Hazard. Mater.*, **163**, 174 (2009).
30. Y. Wang, Y. Zhan, C. Hou, X. He and M. Liu, *J. Taiwan Institute Chem. Engineers*, **7**, 1 (2015).
31. H. Alijan, Z. Shariatini and A. Aroujalian-Mashhadi, *Chem. Eng. J.*, **281**, 468 (2015).
32. V. A. Anagnostopoulos, I. D. Manariotis, H. K. Karapanagioti and C. V. Chrysikopoulos, *Chem. Eng. J.*, **213**, 135 (2012).